A cell-laden microfluidic hydrogel†‡

Yibo Ling,[ab] Jamie Rubin,[c] Yuting Deng,[d] Catherine Huang,[d] Utkan Demirci,[ae] Jeffrey M. Karp[ae] and Ali Khademhosseini*[ae]

Received 25th October 2006, Accepted 5th April 2007
First published as an Advance Article on the web 3rd May 2007
DOI: 10.1039/b615486g

The encapsulation of mammalian cells within the bulk material of microfluidic channels may be beneficial for applications ranging from tissue engineering to cell-based diagnostic assays. In this work, we present a technique for fabricating microfluidic channels from cell-laden agarose hydrogels. Using standard soft lithographic techniques, molten agarose was molded against a SU-8 patterned silicon wafer. To generate sealed and water-tight microfluidic channels, the surface of the molded agarose was heated at 71 °C for 3 s and sealed to another surface-heated slab of agarose. Channels of different dimensions were generated and it was shown that agarose, though highly porous, is a suitable material for performing microfluidics. Cells embedded within the microfluidic molds were well distributed and media pumped through the channels allowed the exchange of nutrients and waste products. While most cells were found to be viable upon initial device fabrication, only those cells near the microfluidic channels remained viable after 3 days, demonstrating the importance of a perfused network of microchannels for delivering nutrients and oxygen to maintain cell viability in large hydrogels. Further development of this technique may lead to the generation of biomimetic synthetic vasculature for tissue engineering, diagnostics, and drug screening applications.

1. Introduction

Biomedical applications ranging from tissue engineering to drug discovery could benefit from the culture of cells within vascularized three-dimensional (3D) extracellular matrix (ECM)-like hydrogels. In tissue engineering, cells seeded within a 3D scaffold are coaxed to deposit their own ECM structure as the scaffold degrades, resulting in a final structure in the shape of the scaffold.[1,2] However, in many large 3D scaffolds, mass transport and nutrient exchange limitations often result in cell necrosis. In contrast, cell screening and drug discovery applications most often utilize cells cultured upon two-dimensional (2D) substrates[3–5] despite the fact that the microenvironment of native tissue consists of complex cell–matrix and cell–soluble factor interactions.[1] This change from the *in vivo* cell microenvironment alters cell function in culture and limits the relevance of diagnostics results.[1] An ideal construct for tissue engineering and diagnostics would provide 3D structural support as well as the exchange of nutrients, waste, and signaling cues.[6]

Microfluidic devices can potentially be used to facilitate the exchange of nutrients and soluble factors in 3D tissue constructs.[7] In microfluidics, the controlled flow of fluids within microscale channels can be used to perform biological analyses and assays.[8,9] Microfluidic devices require minimal reagent consumption, allow for the laminar flow of fluids, and may be used for high-throughput analysis. Currently, microdevices are most commonly fabricated from poly(dimethyl siloxane) (PDMS),[10–13] a flexible silicone rubber that is optically transparent, thereby facilitating analyte visualization. Since PDMS is non-toxic, cells may be cultured on its surfaces or along the walls of its microchannels. However, cells cannot be cultured within the PDMS bulk material. In addition to PDMS, materials such as poly(DL-lactic-*co*-glycolide) (PLGA) and poly(glycerol sebacate) (PGS) have been used to engineer microvasculature within synthetic scaffolds.[14] In these works,[15–17] endothelial and hepatocyte cells were seeded within complex microfluidic channel patterns as a potential method to generate blood vessels and liver constructs for tissue engineering. While PGS and PLGA are biocompatible and biodegradable, potential limitations of this approach include the difficulty of achieving uniform cell seeding, the high volume of the scaffold material which must be degraded, and the 2D surface microenvironment of the scaffolds. The alternative approach presented here aims to overcome these limitations by utilizing cell encapsulation technology.

In contrast to PDMS, PGS, and PLGA, hydrogels consist of 3D crosslinked networks of hydrophilic polymers with mechanical characteristics resembling that of ECM[18–20] and

[a]*Harvard-MIT Division of Health Sciences and Technology, Massachusetts Institute of Technology, Cambridge, MA 02139, USA. E-mail: alik@mit.edu*
[b]*Department of Electrical Engineering and Computer Science, Massachusetts Institute of Technology, Cambridge, MA 02139, USA*
[c]*Department of Chemical Engineering, Massachusetts Institute of Technology, Cambridge, MA 02139, USA*
[d]*Department of Biology, Massachusetts Institute of Technology, Cambridge, MA 02139, USA*
[e]*Center for Biomedical Engineering, Department of Medicine, Brigham and Women's Hospital, Harvard Medical School, Boston, MA 02115, USA*

† This paper is part of a special issue 'Cell and Tissue Engineering in Microsystems' with guest editors Sangeeta Bhatia (MIT) and Christopher Chen (University of Pennsylvania).

‡ Electronic supplementary information (ESI) available: Supplementary Fig. S1–S8. See DOI: 10.1039/b615486g

 This journal is © The Royal Society of Chemistry 2007

thus are amenable for cell encapsulation. These liquid-swelled polymers can be derived from both synthetic (PEG) and natural (alginate, collagen, hyaluronic acid, and agarose)[19] sources. Hydrogels are commonly used in immunoisolation microcapsules,[21,22] as units for scalable bioreactors,[23] and for the tissue engineering of cartilage,[24–26] vasculature[27] and other tissues.[28,29] They exhibit high diffusive permeability to oxygen, nutrients, and other water-soluble metabolites.[30] Recently, calcium alginate[7] and gelatin[31] hydrogels have been used to fabricate microfluidic devices. Also, it was demonstrated that cells could be seeded on the surface of these microchannels. However, to our knowledge, the formation of cell-containing microfluidic hydrogels has not been shown.

Agarose is a thermally reversible polysaccharide consisting of alternating copolymers of (1-3)-linked β-D-galactose and (1-4)-linked (3-6)-anhydro-α-L-galactose[32] that is commonly used for cell encapsulation. It can be induced to melt or gel in a variety of temperatures ranging from 17 °C to 80 °C depending on the molecular weight and chemical modification of the side groups. Cells have been encapsulated in agarose for a variety of applications ranging from biosensing to therapeutics,[21,33] and agarose has been shown to be biocompatible when implanted *in vivo*.[34] While agarose does not directly provide an active attachment substrate, it can be supplemented with collagen or gelfoam to provide attachment sites for anchorage-dependent cells.[32] Also, cells that are encapsulated in agarose hydrogels secrete their own natural ECM.

In this paper, we present a soft lithographic approach for generating cost-effective, cell-laden agarose microfluidic devices. Cells were suspended in low-temperature molten agarose and molded on an SU-8 patterned silicon wafer to generate channel features. Microfluidic channels of different sizes and shapes were fabricated and the diffusion of molecules from the microfluidic channels into the surrounding bulk material was characterized. Cells cultured within agarose microchannels remained viable directly after encapsulation. Also, a zone of high cell viability remained around the microchannels after 3 days of continuous flow of media through the microchannel. This work represents a promising step towards generating biomimetic synthetic vasculature. Additionally, we believe that the principles derived from this work may be extended to other hydrogels such as hyaluronic acid or collagen, which may be superior for some tissue engineering applications.[6,35]

2. Materials and methods

2.1 Cell culture

AML-12 murine hepatocytes were kept at 37 °C in a 95% air/5% CO_2 incubator and maintained in 45% Dulbecco's Modified Eagle Media (DMEM), 45% Ham's F12 Media, and 10% fetal bovine serum (FBS). Confluent flasks of AML-12 cells were passaged and fed every 3–4 days. Murine embryonic stem (ES) cells (R1 strain) were maintained in gelatin treated flasks with media comprised of 15% ES qualified FBS in DMEM knockout media. ES cells were fed daily and passaged every 3 days at a subculture ratio of 1 : 4.

2.2 Agarose mold fabrication

Agarose replicas (1 cm thick, so as to provide sufficient mechanical stability to enable handling) were molded by gelling molten agarose solution on the positive microchannel features of SU-8 patterned silicon masters (Fig. 1). Agarose solutions were generated by heating low gelling temperature agarose (type VII-A, Sigma) in phosphate-buffered saline (PBS) until dissolved. For experiments in which cells were embedded within agarose, 6% agarose (autoclaved/sterilized to dissolve in PBS) was allowed to cool to 70 °C and supplemented with equal volume of cell suspension (cells at controlled densities) to yield a 3% agarose mixture loaded with cells. The molten agarose–cell mixture was then poured onto the silicon master and allowed to gel for 2 h at 25 °C in a sterile tissue culture hood. To form the base of the microchannel, a thin flat slab of agarose was fabricated in a plastic culture dish. The agarose molds were gently peeled from the silicon masters and trimmed to a suitable shape. To make holes for inlets and outlets, a metal feeder wire of ~2 cm in length was used as a guide for insertion of the flexible polyethylene tubing (inner diameter 0.58 mm, outer diameter 0.965 mm, Becton Dickinson). The tubing was then pressed against the feeder wire, forcing the wire out of the hole and fitting the tubing fit place. Finally, the agarose molds were heated on glass slides (75 mm × 25 mm × 1 mm) on a hot plate for 3 s at 71 °C and pressed against one another to form sealed microfluidic channels. The device was allowed to cool for 10 min before fluid was introduced into the channel. These processes involving cells were maintained under sterile conditions.

2.3 Channel flow experiments

To control the flow rate of fluids through the microchannel, the agarose microfluidic device was connected to a syringe pump (AL-1000, World Precision Instruments) via flexible polyethylene tubing. The channel effluent was removed by either collection from an outlet tube connected using a

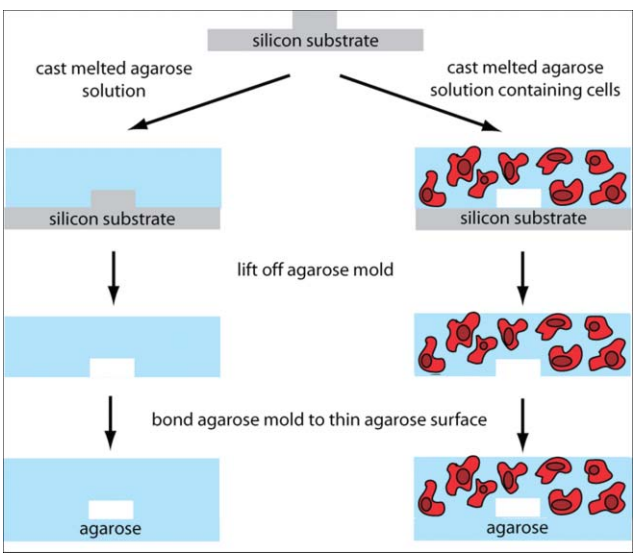

Fig. 1 Schematic of the fabrication of agarose microfluidic devices with (right) and without (left) embedded cells.

procedure similar to that of the inlet tube, or by collection of the effluent directly from the channel outlet.

For experiments in which AML-12 hepatocytes were embedded in microchannels, medium was pumped through 150 μm deep × 800 μm wide channels at a rate of 10 μl min^{-1}. Sterile conditions were maintained throughout the fabrication and operation of the microfluidic device by fabricating and operating the device entirely within a biosafety cabinet. For time dependent studies, the entire apparatus was placed within an incubator at 37 °C and 95% air/5% CO_2 and kept inside a sterilized vessel. To minimize device dehydration (which would presumably affect cell viability), devices were kept within a sterilized vessel maintained in a humidified chamber.

2.4 Sectioning and analytical techniques

Channel flow and diffusion properties were determined by flowing fluorescein isothiocyanate conjugated to bovine serum albumin (FITC-BSA, green fluorescence, excitation/emission = 506/529 nm) through the microchannels at a rate of 100 μl min^{-1}. To quantify diffusion into the surrounding agarose, intensity measurements were calculated from fluorescent images taken every minute for 45 min. These fluorescent intensities, which were taken at a fixed distance from the channel boundary using fixed optical and image capture parameters, were then processed in MATLAB. Specifically, the images were registered, cropped, and averaged over the length of the channel. The fluorescence intensities, assumed to be proportional to the concentration of FITC-BSA, were normalized to the mid-channel intensities of each captured image to account for increasing intensities in progressive images caused by diffusion into the ceiling and floor of the channel.

Initial cell distribution throughout the agarose was evaluated by incubating cells with CFSE (carboxyfluorescein succinimide ester) stain for 15 min prior to encapsulation within the agarose. Cell viability within the microchannels was assessed by applying a live/dead fluorescence assay to slices of agarose microchannels with encapsulated cells. To analyze agarose cross-sections, slices were gently removed with a flat razor blade into ~1 mm thick sections. Live/dead stain was applied directly to the slices, which were incubated for 10 min and visualized under a fluorescent microscope (Nikon, TE2000). Two recognized parameters of cell viability—intracellular esterase activity and plasma membrane integrity—were tracked with the live/dead stain, consisting of PBS solution containing 0.5 μg ml^{-1} calcein AM and 2 μg ml^{-1} ethidium homodimer-1 per 1 ml of PBS. Live cells fluoresced green due to intracellular esterase activity that hydrolyzed the fluorogenic esterase substrate (calcein AM) to a green fluorescent product. Dead cells fluoresced red since their compromised membranes were permeable to the high-affinity red fluorescent nucleic acid stain (ethidium homodimer-1). Percent viability values for Fig. 6B and 6C were calculated by counting the number of live (green) cells and the number of dead (red) cells in a 1.25 mm × 1.25 mm square zone above each channel magnified at 4×. Values were obtained for each control or experimental condition (n = 9 for each value, an average of 230 cells per zone) by dividing the number of live cells by the number of total cells. To average the potential effect of nutrient depletion on cell viability along the axial length of the channel, sections were taken in triplicates from three axial (0 cm, 1.5 cm, 3.0 cm) sections of the channel (resulting in n = 9 for each data point). Percent viability values for Fig. 6C were determined in a similar manner in that the data was binned into 5 vertical zones of 1.25 mm × 0.25 mm each (n = 9 for each value, an average of 46 cells per zone). The exception is that the initial viability value shown in Fig. 6C was obtained from the 1.25 mm × 1.25 mm square zone located above the channel (n = 9). Paired t-tests were used to assess statistically significant differences in viability. Due to potential human error in cell counting we considered $p < 0.005$ to be statistically significant (conservative in comparison to $p < 0.05$ used in many typical biological experiments).

3. Results and discussion

3.1 Channel fabrication

Agarose hydrogels are commonly used in a variety of biological and biomedical applications and are found ubiquitously in electrophoresis applications[36] due to their ability to control the diffusion of biological moieties. In addition, agarose is amenable for soft lithography[37–39] and can be used to micropattern surfaces. The high water content and ECM-like mechanical properties of agarose make it compatible for cell encapsulation.[21] In this work, agarose microfluidic channels were molded on SU-8 patterned silicon wafers, as illustrated in Fig. 1. To seal the two pieces of agarose to form microchannels, they were placed on a glass cover slip and heated on a hot plate so as to slightly melt the bonding interfaces. The two slightly melted surfaces were then annealed to one another to form water tight microchannels. The important parameters for sealing, agarose concentration and heating, are explored in Fig. 2. As expected, low heating resulted in imperfectly sealed and leaky microchannels, while excessive heating resulted in melted channel features. Furthermore, the degree of heating required to melt bulk agarose increases with increasing agarose concentration, a requirement that would presumably have a negative impact on cell viability in cell-laden microfluidic devices. Similarly, the mechanical properties of gelled type VII-A agarose are largely dictated by agarose concentration.[40] While lower concentrations result in moderately transparent but weak bulk materials which fall apart upon even careful handling, higher concentrations result in more opaque (hinders microscopy) yet stiffer bulk materials. Therefore, these parameters (agarose concentration, amount of heating) were optimized for microfluidics fabrication: an agarose concentration of 3% was deemed both sufficiently transparent for imaging and sufficiently robust for careful mechanical handling. Additionally, 3 s of heating at a temperature of 71 °C was found to adequately melt surfaces so as to avoid melting of features while simultaneously improving sealing.

As shown in Fig. 3, agarose microchannels of varying sizes and aspect ratios ranging from 50 μm wide by 70 μm tall (Fig. 3A) to 1000 μm wide by 150 μm tall (Fig. 3B) can be fabricated. The channel in Fig. 3B demonstrates that 3% agarose, at an elastic modulus reported between 19 and 32 kPA,[40,41] is sufficiently rigid to support a large aspect ratio

 This journal is © The Royal Society of Chemistry 2007

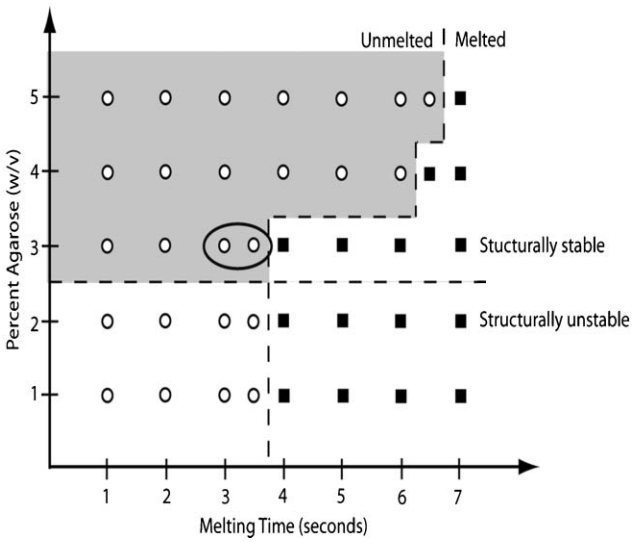

Fig. 2 Diagram for the optimization of agarose concentration and melting time for sealing of surfaces. Circles indicate that channel features were unmelted, and squares indicate melting. Dashed lines mark the boundary between melted and unmelted features and between structurally stable and unstable agarose, where stability was defined as the ability to maintain channel features in the agarose without tearing or deformation. The circled region indicates the chosen experimental conditions.

channel without deformation. Furthermore, the smallest channels (Fig. 3A) demonstrated high fidelity of pattern reproduction, with sharply formed corners and clearly defined edges, suggesting that still smaller channels may be fabricated. This flexibility allows for the potential to generate microchannels spanning the range of actual blood vessels, from capillaries to arteries.

To verify complete channel sealing using the previously described fabrication parameters, FITC-BSA was pumped through the agarose microchannels (Fig. 4). To visualize the diffusivity of molecules through 3% agarose channels, a series of fluorescent images were taken at 1, 5, and 30 min (Fig. 4A).

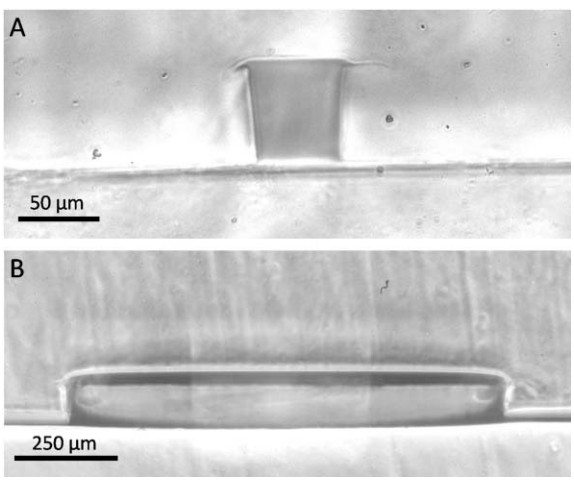

Fig. 3 Light micrograph cross sectional images of agarose channels. Channels (A) 50 μm in width × 70 μm in height and (B) 1 mm in width × 150 μm in depth are depicted.

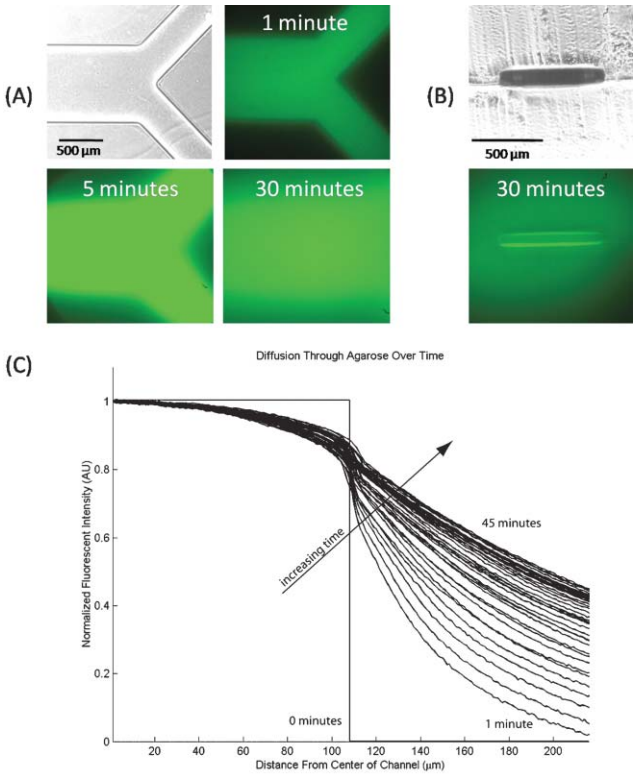

Fig. 4 Characterization of diffusion of FITC-BSA into surrounding agarose. The series of top-down fluorescent images with corresponding phase image in (A) qualitatively depict diffusion with time. In (B) the phase and corresponding fluorescent image of the cross-section of a channel 30 min after FITC-BSA flow are shown. Overlaid intensity profiles (C) are calculated from top-down fluorescent images and plotted for times ranging from 1 min to 45 min.

The immediately visible and sharply defined boundaries of fluorescence in Fig. 4A at 1 minute indicate proper sealing. Diffusion of FITC-BSA into the surrounding channel material is also noticeable in Fig. 4A, taken after 30 min of flow. As previously discussed, high porosity and ease of molecular diffusion are crucial for the viability of encapsulated cells since diffusion facilitates efficient nutrient delivery and waste removal. In addition, the fluorescence intensity of FITC-BSA (MW 69 kDa) as a function of distance away from channels was graphed for 45 min (Fig. 4C). Though the curves have the form of typical diffusion profiles, reliable diffusivity values ($D \sim 6.4 \times 10^{-7}$ cm^2 s^{-1})[42] could not be obtained from the data. This could be due to a number of factors, such as hydraulic pressure from channel flow, evaporation from the agarose surface, and vertical diffusion of FITC-BSA into the ceiling and floor of the channel which skewed the shape of the diffusion profiles.

3.2 Cell encapsulation within agarose

Cells were embedded in agarose microchannels as depicted in Fig. 1. The process is identical to that of microchannel formation without cells, except that cells were added to the agarose prior to molding of the mixture upon the patterned silicon wafer. Live/dead staining immediately upon device fabrication indicated that most cells remained viable throughout the

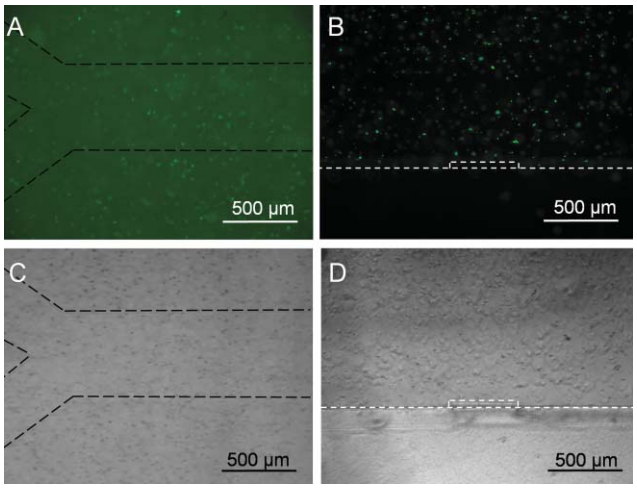

Fig. 5 Fluorescent and brightfield micrographs of CFSE-stained AML-12 cells embedded in an agarose microchannel. Panels A and C show a channel from above while panels B and D show the cross-sectional image of another channel. Dotted lines were added to the images to facilitate visualization at print resolutions.

embedding procedure. The low-gelling temperature of type VII-A agarose (at 1.5% agarose, gelling temperature 26 °C ± 2 °C, melting temperature 65 °C) enabled the cells to be encapsulated within the molten agarose with little exposure to temperatures resulting in cell death (initial cell viability was >80%). A control experiment in which cells were trypsinized and exposed to identical heating conditions (but not embedded within agarose) exhibited similar viability values (~85%), indicating that embedding within agarose does not significantly affect initial cell viability. Fig. 5 shows a microfluidic channel in which mES (A,C) and AML-12 (B,D) cells were embedded within the bulk material of the molded upper layer but not within the bulk material of the flat bottom layer. Light microscopy (Fig. 5C and 5D) and CSFE-labeled fluorescence (Fig. 5A and 5B) images of encapsulation reveal a fairly homogeneous distribution of cells throughout the molded bulk agarose material. Further observation of sections of different channel regions (not shown) indicated that the cells were homogeneously distributed throughout the rest of the device as well.

3.3 Viability of encapsulated cells

To assess the potential of cell-laden agarose microfluidics for extended cell encapsulation, viability assays were conducted over time with AML-12 murine hepatocytes encapsulated at a density of 2×10^6 cells ml^{-1} within the bulk material of agarose microchannels. Though the initial viability of 3T3 fibroblasts and mES cells were also verified (data not shown), hepatocytes were chosen in the device characterization experiments discussed below for their potential applications in engineering liver constructs and toxicity assays. Upon formation of microchannels, cell culture media was pumped through the channels for up to three days. The flow rate of 10 μl min^{-1} yielded a shear stress value of 1.18 Pa (using a previously described method)[43] and was chosen because it falls within the physiological shear stress range of mammalian

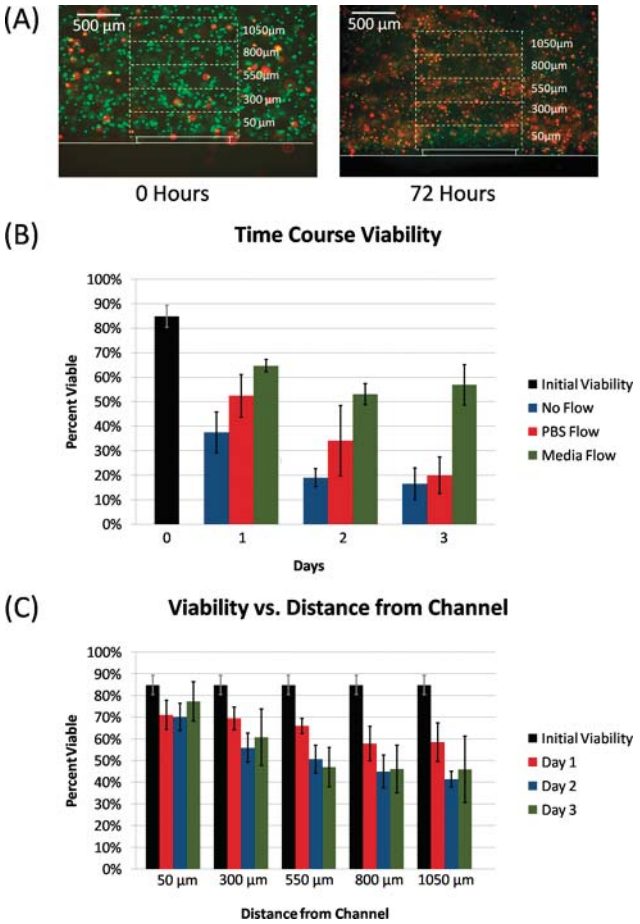

Fig. 6 Quantification of cell viability in the agarose microchannels over time. The images in (A) are representative live/dead staining of AML-12 murine hepatocytes encapsulated in agarose channels after 0 (left) and 3 days (right). Rectangular regions demarcated by dashed white lines correspond to ~250 μm thick zones where the labeled height values correspond to the mean distance of each zone above the channel floor. The graph in (B) plots percent viability values for initial (n = 27) as well as for up to three days under 2 control conditions (no flow, PBS flow) and experimental media flow conditions (n = 9 for all three conditions). In part (C) the time course viability under experimental media flow conditions for 1.25 mm × 0.25 mm zones of progressively increasing distances (50 μm, 300 μm, 550 μm, 800 μm, 1050 μm) from the channel are shown (n = 9). Error bars span one standard deviation from the mean.

arteries (0.51–5.0 Pa in rabbits).[44] Vertical channel slices were collected each day and stained to evaluate cell viability (Fig. 6A).

As shown in the left panel of Fig. 6A, the majority of cells were viable upon initial device fabrication. Control experiments that exposed trypsinized but unencapsulated cells to identical processing temperatures (as high as 70 °C, including cooling time) exhibited similar viability values (~85%). There is no noticeable cell death at the adherent boundary between the two agarose pieces, indicating that the brief surface heating (71 °C for 3 s, to facilitate bonding of the two pieces) did not cause noticeable cell death. Therefore, higher agarose concentrations, which require more heating to facilitate bonding, may also be tolerable for cell viability.

This journal is © The Royal Society of Chemistry 2007

Due to processing requirements (cell-loaded devices were set for 2 hours to facilitate agarose gellation), the devices were fabricated with media (at 50%) to prevent compromise of cell viability. However, this introduced the likelihood that cell viability would initially be partially maintained by pre-loaded media rather than delivered media. To assess the effect of this phenomenon, no-flow control experiments were performed (Fig. 6B). It appears that the media used during device fabrication supports a fraction of cells up to 3 days. In addition, data gathered under experimental conditions in which media was continuously pumped through the device shows statistically significant increases in viability between experimental and no-flow control conditions for day 1, day 2, and day 3. By day 3, the difference between experimental and no-flow control conditions was dramatic (>55% for experimental, <20% for no-flow control). Additionally, while there are significant drops in viability between each day up to day 2, there was no significant difference in the viability of control experiments between days 2 and 3.

To assess the impact of waste removal on cell viability an additional set of PBS flow experiments were performed. From the data shown in Fig. 6B, while there does appear to be statistically significant differences in time-course cell viability for this condition when compared to the no-flow controls on days 1 and 2, this difference disappears by day 3. It is important to note that we cannot in these experiments segregate the effect of waste removal from dilution of the pre-loaded media; however, one reasonable explanation for these results is that the initial (days 1 and 2) increases in viability are due to waste removal, which becomes insignificant by day 3. Therefore, the effect of waste removal in improving cell viability in this system does appear to overwhelm the detrimental effect of nutrient dilution in the first 2 days.

No significant variations in viability with respect to distance above the channel were observed immediately after the encapsulation process. Over time, cells further from the microchannel gradually lost viability, as shown in a representative image from day 3 in the right portion of Fig. 6A in which zones further from the channel may be qualitatively compared to the zones that are closer. To quantitatively assess the effect of distance above the microchannel as a function of time under experimental conditions, the percent viability of zones roughly 1.25 mm × 0.25 mm (visualized in Fig. 6A by dashed white lines) centered atop and binned at progressively greater distances above the channel are plotted individually in Fig. 6C. This data shows significantly larger drops in viability for regions at greater (1050 μm) distances from the channel. In the region closest to the channel (50 μm) while there is a small (in comparison to regions at greater distances) but significant drop in viability on day 1 in comparison to initial viability, no further significant differences are found between day 1 and 2 or between 2 and 3. Furthermore, these results indicate while cells at greater distances from the channel do lose viability, they also remained significantly more viable than control condition counterparts. This phenomenon was likely the result of diffusion limitations within the bulk agarose, preventing adequate nutrient and waste exchange to cells embedded at larger distances from the microchannel. This property is shared by the natural vasculature of tissues (capillaries in human tissues are typically found ~200 μm apart).

Finally, to assess the possibility of nutrient depletion along the axial direction (direction of flow) of the channel, individual slices from devices with channels 3 cm in length collected from the beginning (0 cm), middle (1.5 cm), and end (3.0 cm) of each channel are plotted individually. Both PBS control (Fig. S1–S3, ESI‡) and experimental media flow (Fig. S4–S8, ESI‡) conditions are presented. These detailed results are presented in the ESI‡ but essentially indicate that nutrient depletion, or alternatively waste accumulation, did not appear to impact cell viability within statistical error along the length of the channel used. This result is expected since the residence time of any particular volume of media within the channel (which can be modulated by adjusting flow rate) is less than half a minute. However, limitations due to axial nutrient depletion and waste accumulation would be expected to affect cell viability for longer channels and slower flow rates.

3.4 Future work

The lithographic approach presented here should be compatible with any number of agarose mixtures or other hydrogels. To overcome the absence of an attachment matrix, the agarose could be supplemented with ECM additives such as collagen or gelfoam. Signaling molecules may also be incorporated within the hydrogel, either dissolved within the liquid phase or conjugated to agarose *via* a Williams ether synthesis (attachable to the amine group of the ligand).[45] Alternatively, the use of natural ECM molecules such as hyaluronic acid or collagen may provide a more chemically and mechanically *in vivo*-like environment, leading to superior assimilation of the resulting structures into the host tissue and cell migration and proliferation within the hydrogel matrix.

Cell-laden microfluidic hydrogels can also be scaled up. In this process, biomimetic vascular patterns may be fabricated and stacked layer-by-layer, one upon another to generate multi-layer vascularization in multiple discrete planes. The thickness of each plane may need to be optimized for cell viability throughout the volume of the construct (data here shows a zone of high viability up to 200 μm away from the channels, suggesting channels 400 μm apart vertically). However, such an approach would require the future development of more mechanically stable materials (possibly alternative materials or agarose with additives) that can be fabricated and handled as very thin layers (currently, devices are 1+ cm thick). While much work needs to be performed in characterizing the mass transport of macromolecules from microfluidic channels into the surrounding material, such an approach could be used to engineer the transport of nutrients, wastes, and soluble factors to complex macroscale 3D cellular constructs.

4. Conclusion

In summary, we have developed a soft lithographic technique for fabricating cell-laden agarose microfluidic devices. Fully sealed channels of different aspect ratios were replicated with high pattern fidelity, demonstrating that agarose is a suitable material for microfluidic applications. In addition, cells were

homogeneously distributed in agarose, and the delivery of media through the channel allowed cells in close proximity to the channels to remain viable for at least 3 days. This simple method may be useful for diagnostic tools and for generating synthetic vasculature within tissue engineered constructs.

Acknowledgements

The authors would like to acknowledge funding from The Coulter Foundation, the Center for Integration of Medicine and Innovative Technology (CIMIT) and the Charles Stark Draper Laboratory. We also thank Dylan Wright and Danilo Scepanovic for helpful discussions. YL is supported by a NDSEG fellowship.

References

1 A. Khademhosseini, R. Langer, J. Borenstein and J. P. Vacanti, *Proc. Natl. Acad. Sci. U. S. A.*, 2006, **103**, 2480–2487.
2 R. Langer and J. P. Vacanti, *Science*, 1993, **260**, 920–926.
3 J. C. Love, J. L. Ronan, G. M. Grotenbreg, A. G. van der Veen and H. L. Ploegh, *Nat. Biotechnol.*, 2006, **24**, 703–707.
4 S. A. Fuller, M. Takahashi and J. G. R. Hurrell, *Current Protocols in Molecular Biology*, John Wiley & Sons, Inc., New York, 2003.
5 W. M. Yokoyama, *Current Protocols in Molecular Biology*, John Wiley & Sons, New York, 1995.
6 J. Yeh, Y. Ling, J. M. Karp, J. Gantz, A. Chandawarkar, G. Eng, J. Blumling Iii, R. Langer and A. Khademhosseini, *Biomaterials*, 2006, **27**, 5391–5398.
7 M. Cabodi, N. W. Choi, J. P. Gleghorn, C. S. Lee, L. J. Bonassar and A. D. Stroock, *J. Am. Chem. Soc.*, 2005, **127**, 13788–13789.
8 C. Hansen and S. R. Quake, *Curr. Opin. Struct. Biol.*, 2003, **13**, 538–544.
9 D. J. Beebe, G. A. Mensing and G. M. Walker, *Annu. Rev. Biomed. Eng.*, 2002, **4**, 261–286.
10 S. Takayama, J. C. McDonald, E. Ostuni, M. N. Liang, P. J. A. Kenis, R. F. Ismagilov and G. M. Whitesides, *Proc. Natl. Acad. Sci. U. S. A.*, 1999, **96**, 5545–5548.
11 A. D. Stroock, S. K. W. Dertinger, A. Ajdari, I. Mezic, H. A. Stone and G. M. Whitesides, *Science*, 2002, **295**, 647–651.
12 D. J. Beebe, J. S. Moore, J. M. Bauer, Q. Yu, R. H. Liu, C. Devadoss and B. H. Jo, *Nature*, 2000, **404**, 588–590.
13 P. J. A. Kenis, R. F. Ismagilov and G. M. Whitesides, *Science*, 1999, **285**, 83–85.
14 K. King, C. Wang, M. Kaazempur-Mofrad, J. Vacanti and J. Borenstein, *Adv. Mater.*, 2004, **16**, 2007–2012.
15 J. T. Borenstein, H. Terai, K. R. King, E. J. Weinberg, M. R. Kaazempur-Mofrad and J. P. Vacanti, *Biomed. Microdev.*, 2002, **4**, 167–175.
16 C. J. Bettinger, E. J. Weinberg, K. M. Kulig, J. P. Vacanti, Y. Wang, J. T. Borenstein and R. Langer, *Adv. Mater.*, 2006, **18**, 165–169.
17 C. Fidkowski, M. R. Kaazempur-Mofrad, J. Borenstein, J. P. Vacanti, R. Langer and Y. Wang, *Tissue Eng.*, 2005, **11**, 302–309.
18 N. Peppas, J. Z. Hilt, A. Khademhosseini and R. Langer, *Adv. Mater.*, 2006, **18**, 1345–1360.
19 K. Y. Lee and D. J. Mooney, *Chem. Rev.*, 2001, **101**, 1869–1879.
20 J. A. Rowley, G. Madlambayan and D. J. Mooney, *Biomaterials*, 1999, **20**, 45–53.
21 A. Khademhosseini, M. H. May and M. V. Sefton, *Tissue Eng.*, 2005, **11**, 1797–1806.
22 S. Lahooti and M. V. Sefton, *Cell Transplant.*, 2000, **9**, 785–796.
23 S. M. Dang, M. Kyba, R. Perlingeiro, G. Q. Daley and P. W. Zandstra, *Biotechnol. Bioeng.*, 2002, **78**, 442–453.
24 S. J. Bryant, R. J. Bender, K. L. Durand and K. S. Anseth, *Biotechnol. Bioeng.*, 2004, **86**, 747–755.
25 S. J. Bryant and K. S. Anseth, *J. Biomed. Mater. Res., Part A*, 2003, **64**, 70–79.
26 J. Elisseeff, W. McIntosh, K. Anseth, S. Riley, P. Ragan and R. Langer, *J. Biomed. Mater. Res.*, 2000, **51**, 164–171.
27 B. Mann, A. Gobin, A. Tsai, R. Schmedlen and J. West, *Biomaterials*, 2001, **22**, 3045–3051.
28 D. L. Hern and J. A. Hubbell, *J. Biomed. Mater. Res.*, 1998, **39**, 266–276.
29 J. A. Burdick, M. N. Mason, A. D. Hinman, K. Thorne and K. S. Anseth, *J. Controlled Release*, 2002, **83**, 53–63.
30 K. T. Nguyen and J. L. West, *Biomaterials*, 2002, **23**, 4307–4314.
31 A. Paguirigan and D. J. Beebe, *Lab Chip*, 2006, **6**, 407–413.
32 H. Uludag, P. De Vos and P. A. Tresco, *Adv. Drug Deliv. Rev.*, 2000, **42**, 29–64.
33 K. S. Jones, M. V. Sefton and R. M. Gorczynski, *Transplantation*, 2004, **78**, 1454–1462.
34 B. Rahfoth, J. Weisser, F. Sternkopf, T. Aigner, K. von der Mark and R. Brauer, *Osteoarthritis Cartilage*, 1998, **6**, 50–65.
35 A. Batorsky, J. Liao, A. W. Lund, G. E. Plopper and J. P. Stegemann, *Biotechnol. Bioeng.*, 2005, **92**, 492–500.
36 P. Borst, *IUBMB Life*, 2005, **57**, 745–747.
37 D. B. Weibel, A. Lee, M. Mayer, S. F. Brady, D. Bruzewicz, J. Yang, W. R. Diluzio, J. Clardy and G. M. Whitesides, *Langmuir*, 2005, **21**, 6436–6442.
38 M. M. Stevens, M. Mayer, D. G. Anderson, D. B. Weibel, G. M. Whitesides and R. Langer, *Biomaterials*, 2005, **26**, 7636–7641.
39 G. T. Franzesi, B. Ni, Y. Ling and A. Khademhosseini, *J. Am. Chem. Soc.*, 2006, **128**(47), 15064–15065.
40 Q. Chen, B. Suki and K. N. An, *J. Biomech. Eng.*, 2004, **126**, 666–671.
41 M. Benkherourou, C. Rochas, P. Tracqui, L. Tranqui and P. Y. Gumery, *J. Biomech. Eng.*, 1999, **121**, 184–187.
42 A. Pluen, P. A. Netti, R. K. Jain and D. A. Berk, *Biophys. J.*, 1999, **77**, 542–552.
43 O. C. Farokhzad, A. Khademhosseini, S. Jon, A. Hermmann, J. Cheng, C. Chin, A. Kiselyuk, B. Teply, G. Eng and R. Langer, *Anal. Chem.*, 2005, **77**, 5453–5459.
44 T. A. R.S. Renemana and A. P. G. Hoeksb, *J. Vas. Res.*, 2006, **43**, 251–269.
45 J. K. Inman in *Affinity Chromatography—a practical approach*, ed. P. D. G. Dean, W. S. Johnson and F. A. Middle, IRL Press Limited, Oxford, 1985, p. 53.

 This journal is © The Royal Society of Chemistry 2007